Ocean Surface Wind and Stress

WT Liu and X Xie, Jet Propulsion Laboratory, California Institute of Technology, Pasadena, CA, United States

Introduction

Wind is air in motion as part of the atmospheric circulation. It is a vector with a magnitude (speed) and a direction. Ocean surface stress is the turbulent transfer of momentum between the ocean and the atmosphere and is another vector closely related to wind. The needs for wind and stress are summarized in "Significance" section. Surface turbulence is generated/suppressed by wind shear (difference between wind and current) and buoyancy (vertical density stratification resulting from temperature and humidity gradients). There were almost no in situ stress measurements except in dedicated field campaigns. The stress estimates we used were almost entirely derived from wind measurements through a drag coefficient, as described in "Relating Wind and Stress" section. Wind variation has been taken as stress variation.

There are space-borne active and passive microwave sensors that provide surface wind data under clear and cloudy conditions, day and night, over global oceans; the most established wind vector sensor is the scatterometer, which is described in "Measurements from Space" section. Although the scatterometer has been promoted as a wind sensor, its measurement is more closely related to stress. Two examples are given to bring out the unique capability of the scatterometer in measuring stress; one is under the strong wind of tropical cyclones (TC), where shear production of turbulence dominates ("Under Tropical Cyclone" section), and another is over mesoscale eddies at temperature fronts, where buoyancy production is also important ("Over Ocean Fronts and Eddies" section).

Significance

Just a few decades ago, almost all ocean wind measurements came from merchant ships. However, the quality and geographical distribution of these wind reports were uneven. Today, operational numerical weather prediction (NWP) also gives us wind information, but NWP depends on models, which are limited by our knowledge of the physical processes and the availability of data. Ocean wind is strongly needed for marine weather forecast and to avoid shipping hazards. Space-based wind measurements have been assimilated into operational NWP and used routinely in national centers for marine warning and forecasting. Surface wind convergence brings moisture and latent heat that drives deep convection and fuels TC. The significance of wind measurement is clearly felt, for example, when a TC suddenly intensifies and changes course or when the unexpected delay of monsoon brings drought.

Wind-induced stress drives ocean current (ageostrophic component) and wave generation. The two-dimensional stress field is needed to compute the divergence and curl (vorticity) that control the vertical mixing. The mixing brings short-term momentum and heat trapped in the surface mixed layer into the deep ocean, where they are stored over time. It brings nutrients to the surface, where there is sufficient light for photosynthesis, and affects the sinking of carbon sequestered as net primary production to the deep. The horizontal currents, driven in part by stress, distribute the stored heat and carbon in the ocean. Stress affects the turbulent transfer of heat, moisture, and gases between the ocean and the atmosphere and is critical in understanding and predicting weather and climate changes.

 http://dx.doi.org/10.1016/B978-0-12-409548-9.10399-9

Relating Wind and Stress

Before the scatterometers, there were almost no stress measurement except in dedicated field campaigns and the stress estimates we used were almost entirely derived from wind measurements. A drag coefficient (C_D) is used to derive stress (τ) from wind (U) at a reference height, and it is defined by

$$\tau = \rho C_D (U - U_S)^2 \tag{1}$$

where U_s is the surface current and ρ is the air density. Although we include U_s in Eq. (1), it is usually ignored because its magnitude is small compared to wind. For a moderate range of wind speed, C_D has been well studied and derived largely in field campaigns (Smith, 1980; Large and Pond, 1981). Over large-scale open-ocean, it is found to increase almost linearly with wind speed. Liu et al. (1979) provided the first bulk parameterization method based on flux–profile relations (or similarity functions), including stability effects (the balance between wind shear and buoyancy production of turbulence). Secondary factors, like sea states, swell, and spray from breaking waves, are not included, and they contribute to the uncertainties of the C_D.

The bulk parameterization methods and the similarity functions are valid in the atmospheric surface layer (around 10 m from the surface), where the flux divergence is small, and the scaling depth is the Obukhov length, governed only by the ratio of buoyance to shear turbulence production. Further up in the atmospheric boundary layer (around 1 km from the surface), other forces, such as pressure gradient force, Coriolis force, baroclinicity, cloud entrainment, horizontal temperature advection, and secondary flow, become more effective. Brown and Liu (1982) gave a simple boundary layer perspective to relate the geostrophic winds at top to the surface stress at the bottom. Geostrophic winds result from a balance between Coriolis and pressure gradient forces, with cyclonic rotation around the low-pressure centers and opposite rotation over high pressure centers. Frictional force, baroclinicity, and other factors are added to change the geostrophic wind, with realistic turning into and away from pressure center down the boundary layer to the surface layer where turbulent transport dominates.

As discussed by Liu et al. (1979), C_D does not change linearly with wind speed at low wind speed range, as the surface becomes smooth. There are large uncertainties of the drag coefficient at high winds because of the lack of stress measurement.

Measurements from Space

The ocean interacts with the atmosphere in nonlinear ways and processes at one scale affect processes at other scales. Adequate coverage can only be achieved from the vantage point of space. The microwave scatterometer is the best-established instrument dedicated to measure surface wind and stress vector (e.g. Liu, 2002). **Table 1** lists past and current scatterometers whose data are available to the public. The primary functions of the radar altimeter, the synthetic aperture radar, and the microwave radiometer are not wind-stress measurements, but they give wind speed as a secondary product. Wind speed, even without direction, is important, and wind speed from these sensors can be applied with directional information derived from other means. Both active and passive wind sensors in the past were summarized by Liu and Xie (2006). The polarimetric radiometer was found to be sensitive also to both wind direction and wind speed. A good example is the application of polarimetric radiometer, WindSat, data in the TC study described in "Under Tropical Cyclone" section.

The scatterometer sends microwave pulses to the Earth's surface and measures the power backscattered from the surface roughness. Over the ocean, the surface roughness is largely due to the small centimeter waves (including capillary waves), which are believed to be in equilibrium with the surface stress. The initial geophysical model functions relate measured normalized radar cross section σ_o to the frictional velocity $U_* = (\tau/\rho)^{1/2}$, representing kinematic stress (Jones and Schroeder, 1978). The expression is

$$\sigma_o = f(U_*, \chi, \theta, p) \tag{2}$$

Table 1 Past and current scatterometers

Instrument	*Time period*	*Space agency*
Seasat	6/1978–10/1978	NASA
ERS-1	7/1991–4/1996	ESA
ERS-2	4/1995–6/2003	ESA
NSCAT	8/1996–6/1997	NASA/NASDA
QuikSCAT	6/1999–11/2009	NASA
SeaWinds	12/2002–10/2003	NASA/NASDA
ASCAT-A	10/2006–present	EUMETSAT
Oceansat2	9/2009–2/2014	ISRO
ASCAT-B	9/2012–present	EUMETSAT
RapidScat	9/2014–8/2016	NASA
Scatsat	9/2016–present	ISRO

where χ is the relative azimuth angle between the plane of incidence of the radar beam and the stress direction, θ is the incidence angle (relative to nadir), and p represents the polarization (Jones and Schroeder, 1978). The data products of the first operational scatterometer, SEASAT, were validated against measured stress (Liu and Large, 1981).

At $\theta > 20°$, the σ_o is governed by Bragg scattering, and it increases with U_*. The backscatter is governed by the in-phase reflections from surface waves. The symmetry of backscatter with stress direction requires observations at multiple χ to resolve the directional ambiguity. Because of the uncertainties in the retrieval algorithm and noise in the backscatter measurements, the problem with directional ambiguity was not entirely eliminated even with three azimuthal looks in the scatterometers launched after Seasat. A median filter iteration technique has been commonly used to remove the directional ambiguity.

Because the public is more familiar with wind than stress, and there are more wind measurements than stress measurements for calibration and validation, the equivalent neutral wind U_N has been used as the geophysical product. U_N, by definition, has an unambiguous relation with surface stress, while the relation between actual wind and surface stress depends also on atmospheric stability. The derivation of U_N from in situ wind measurements by removing the stability effect is described in Liu and Xie (2013). The computational procedure (Liu and Tang, 1996) has been used in algorithm development and calibration of all scatterometers launched by NASA. If derived correctly, U_N and U_* can be viewed as stress in wind unit.

Under Tropical Cyclone

The difficulty of retrieving strong winds from the scatterometer, as illustrated in **Fig. 1**, was demonstrated in several studies (e.g., Liu et al., 2010; Liu and Xie, 2013). QuikSCAT (see **Table 1**) σ_o are compared with collocated H^*wind speed that is operationally produced by the Hurricane Research Division at the Atlantic Oceanographic and Meteorological Laboratory (Powell et al., 1998).

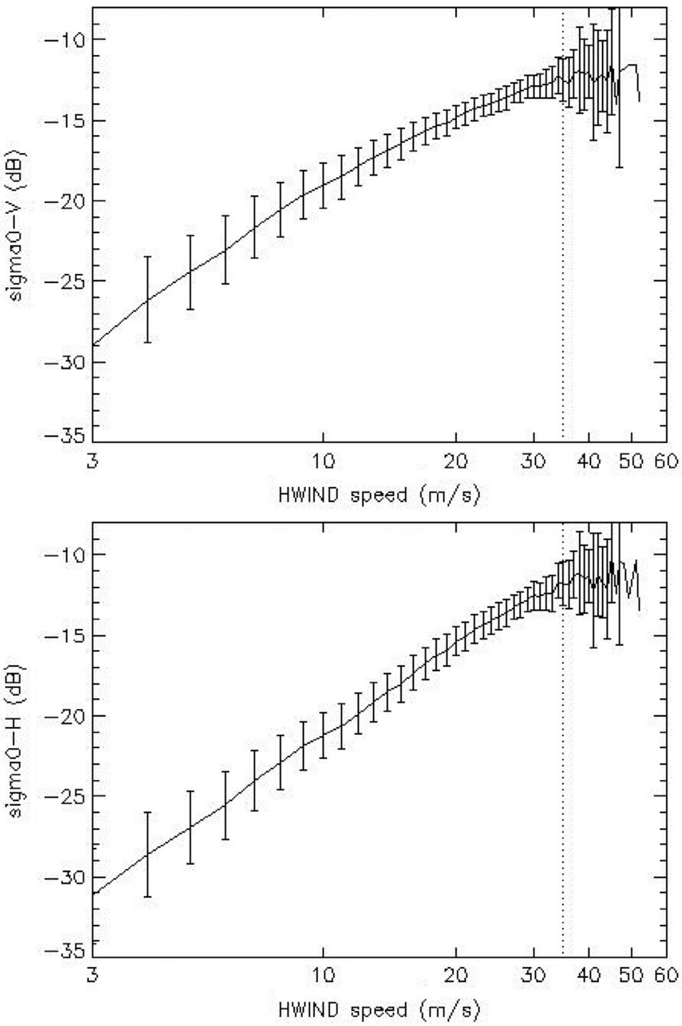

Fig. 1 Normalized radar cross section at two polarization measured by QuikSCAT for 12 hurricanes as a function of colocated surface wind provided by the National Hurricane Center.

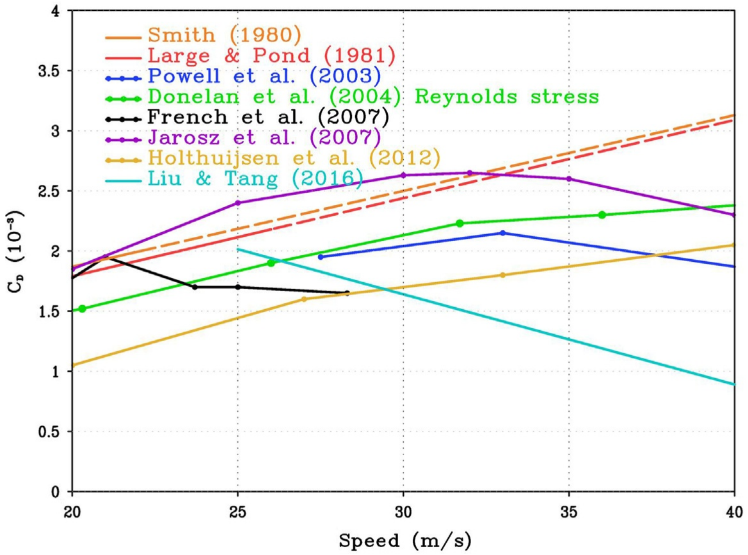

Fig. 2 Drag coefficient as a function of wind speed computed from stress measured by QuikSCAT, with a linear regression of the combined bin averages. Drag coefficients of past studies are plotted for comparison.

H^*wind was produced from surface winds within a time window of TC passes from various sources, projected to a level of 10-m and linearly interpolated to complete a wind field representative of the entire cyclone. In **Fig. 1**, data for the 12 TC in North Atlantic in the 2005 seasons, excluding those with over 10% chances of rain, were examined.

In moderate winds ($U < 30\ \mathrm{ms}^{-1}$), the logarithm of σ_o (in dB) increases almost linearly with the logarithm of wind speed. At strong winds ($U > 30\ \mathrm{ms}^{-1}$), however, σ_o increases at a much slower rate with increasing wind speed. When the model function developed over the moderate wind range is applied to the strong winds, an underestimation of wind speed results. Strong efforts have been made to adjust the model function (slope in **Fig. 1**) in strong winds, but there are not sufficient in situ measurements available to give credible results. The variations caused by change in azimuth angle should be a major part of the error bars. There were efforts to find a remote-sensing solution, i.e., to find the right channel (combination of polarization, frequency, incidence angle) that would be more sensitive to the increase of strong winds (Esteban-Fernandez et al., 2006; Fois et al., 2015). However, such potential has not been tested out in operational space-borne sensors.

Liu et al. (1979) first postulated that, in a rough sea, under a moderate range of winds (between 3 and 20 ms^{-1}), the transfer coefficients of sensible and latent heat do not increase with wind speed because of molecular constraint at the interface, while C_D, the transfer coefficient for momentum, may still increase because momentum is transported by form drag over the waves. Emanuel (1995) argued, from theoretical and numerical model results, that the scenario of Liu et al. (1979) could not hold at the strong wind regime of a TC. To attain the wind strength of a TC, the energy dissipated by drag could not keep increasing while the energy fed by sensible and latent heat does not increase with wind speed. His argument puts limit on the increase of C_D as a function of wind speed. The postulation that the increase of C_D with wind speed will level off or decrease at TC scale winds was supported by the results of many subsequent studies. In **Fig. 2**, examples of C_D for TC as a function of wind speed are shown together with the extension of C_D established for moderate winds (Large and Pond, 1981; Smith, 1980). Donelan et al. (2004) measured stress in a laboratory. Powell et al. (2003) derived stress from the gradient of wind profile measured by dropsondes assuming a logarithmic distribution. French et al. (2007) measured stress by eddy correlation method in an aircraft, but not in very high winds (not shown). Recently, Jarosz et al. (2007) estimated stress from current measurements, Holthuijsen et al. (2012) also addressed wave breaking, and Bell et al. (2012) based their estimates on angular momentum balance. Soloviev et al. (2014) give a more recent review of C_D values and postulations on its behavior at high winds. Despite all the innovative stress estimates in TC, the large spread of the values in the figure shows clearly the unsatisfactory stage of our present knowledge.

Liu and Tang (2016) postulated that the microwave backscatter from ocean surface roughness, which is in equilibrium with local stress, does not distinguish weather systems. The algorithm that relates σ_o to surface roughness was initially developed based on theory, artificial waves, and stationary roughness, independent of surface aerodynamics (e.g. Wright, 1968; Brown, 1978) and did not consider weather change. The reduced sensitivity of scatterometer wind retrieval algorithm under the strong wind is an air–sea interaction problem that is caused by flow separation and a change in the behavior of the drag coefficient and not a sensor problem. Under this assumption, they applied a stress retrieval algorithm developed over a moderate wind range to retrieve stress under the strong winds of TCs. Over a moderate wind range, the abundant wind measurements and more established drag coefficient value allow sufficient stress data to be computed from wind to develop a stress retrieval algorithm for the scatterometer. Using almost a million coincident stress and wind pairs, they showed that the drag coefficient decreases with wind speed at a much steeper rate than previously revealed, for wind speeds over 25 ms^{-1}, as shown in **Fig. 2**. The study clearly showed that stress does not increase as fast as wind in TC. While there are strong wind gradients through the eye-wall, the ocean surface under these high wind regions may be rather smooth. The stress retrieved from the scatterometer implies that the ocean applies less drag to inhibit TC intensification and the TC causes less ocean mixing and surface cooling than previous studies indicated.

Over Ocean Fronts and Eddies

Current Effect

Stress does not depend on wind alone but is affected by ocean current (Eq. 2). Kelly et al. (2001) discussed current effects on wind measurements in the tropical ocean. Pacanowski (1987) demonstrated the current effect on momentum transport in ocean general circulation model three decades ago. Several numerical experiments have shown that stress computed with surface current in addition to wind reduces the overall kinetic energy transfer from the wind to the ocean (Duhaut and Straub, 2006; Hogg et al., 2009). The current effect is most evident in scatterometer observations of ocean eddies associated with the meanders of the Agulhas and Kuroshio Extension Currents (Liu et al., 2007; Liu and Xie, 2008). It is well known that the ocean fronts and the associated mesoscale eddies have very high kinetic energy.

In **Fig. 3**, the drifter data reveal that the Kuroshio Current separates from the coast of Japan at about 36°N to form the Kuroshio Extension across the Pacific. Two quasipermanent meanders, with SST ridges at 144°E and 150°E, are examined in this study as described by Liu and Xie (2008). A cyclonic current causes divergence and upwelling of cold water, while an anticyclonic current causes downwelling. Cold SST, as measured by AMSR-E, is located with the cyclonic current; warm SST is located with anticyclonic currents, as shown in the figure. Although SST data are averaged only over a three-year period (June 2002–May 2005) and surface currents are averaged over a five-year period (January 2000–December 2004), the centers of their anomalies are approximately collocated. Drifter data are sparse and it takes 5 years to cover the region adequately. To separate the mesoscale features from large-scale spatial gradient, a two-dimensional filter was applied to the monthly means.

The filtered data clearly show cyclonic currents around cold water while anticyclone current over warm water in **Fig. 4A**. The cold and warm centers are marked by crosses and circles shown in **Fig. 3**. QuikSCAT observed that U_N (or stress) have opposite vorticity as the surface current, as shown in **Fig. 4B**. Stress depends on the vector difference between wind and current (Eq. 2). With nonrotating wind overheads, stress should have a component rotating in the opposite direction to the current, as postulated by Park et al. (2006), with reference to Gulf Stream rings. The sign of U_N vorticity in opposite to that of surface current clearly indicates that the scatterometer measures stress rather than wind and implies that the stress spins down the ocean eddies. While **Fig. 4** shows the annual mean distribution, **Fig. 5** shows consistent month-to-month variation of U_N vorticity location related to the eddies.

Temperature Effect

When the first QuikSCAT data came back in 1999, the science team was surprised to see that the scatterometer signal in the equatorial Pacific propagates westward with the sea surface temperature (SST) front of the tropical instability waves in the area where we expected to see steady trade winds (Liu et al., 2000; Chelton et al., 2001). We also found out that such coincident propagation was previously observed by Xie et al. (1998) in European Research Satellite data. Since then, the spatial coherence between scatterometer measurements and SST has been observed over many locations and under various atmospheric

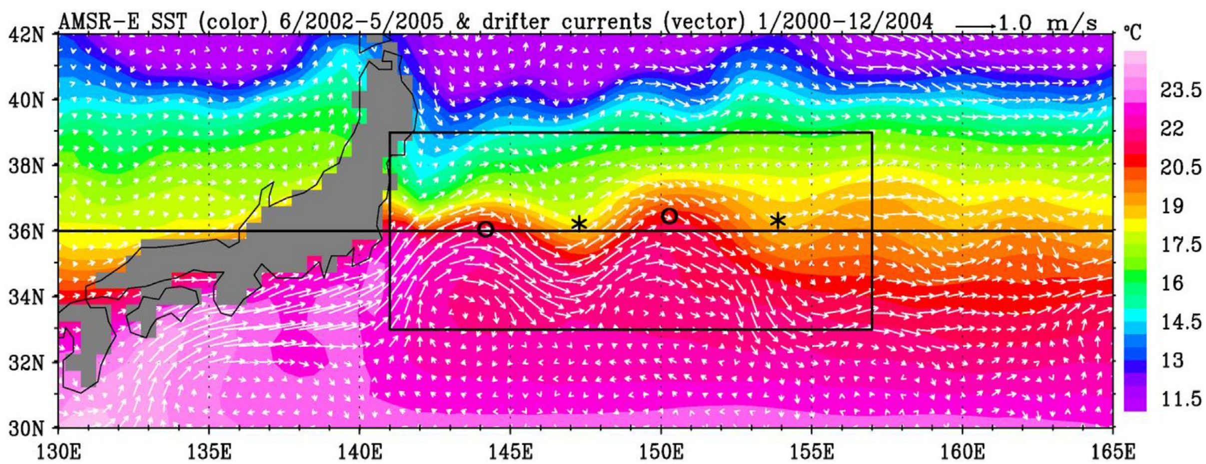

Fig. 3 Ocean surface current measured by Lagrangian drifters (*white arrows*) superimposed on SST (color, °C) from AMSR-E. *Circles and stars* represent centers of warm and cold SST anomalies.

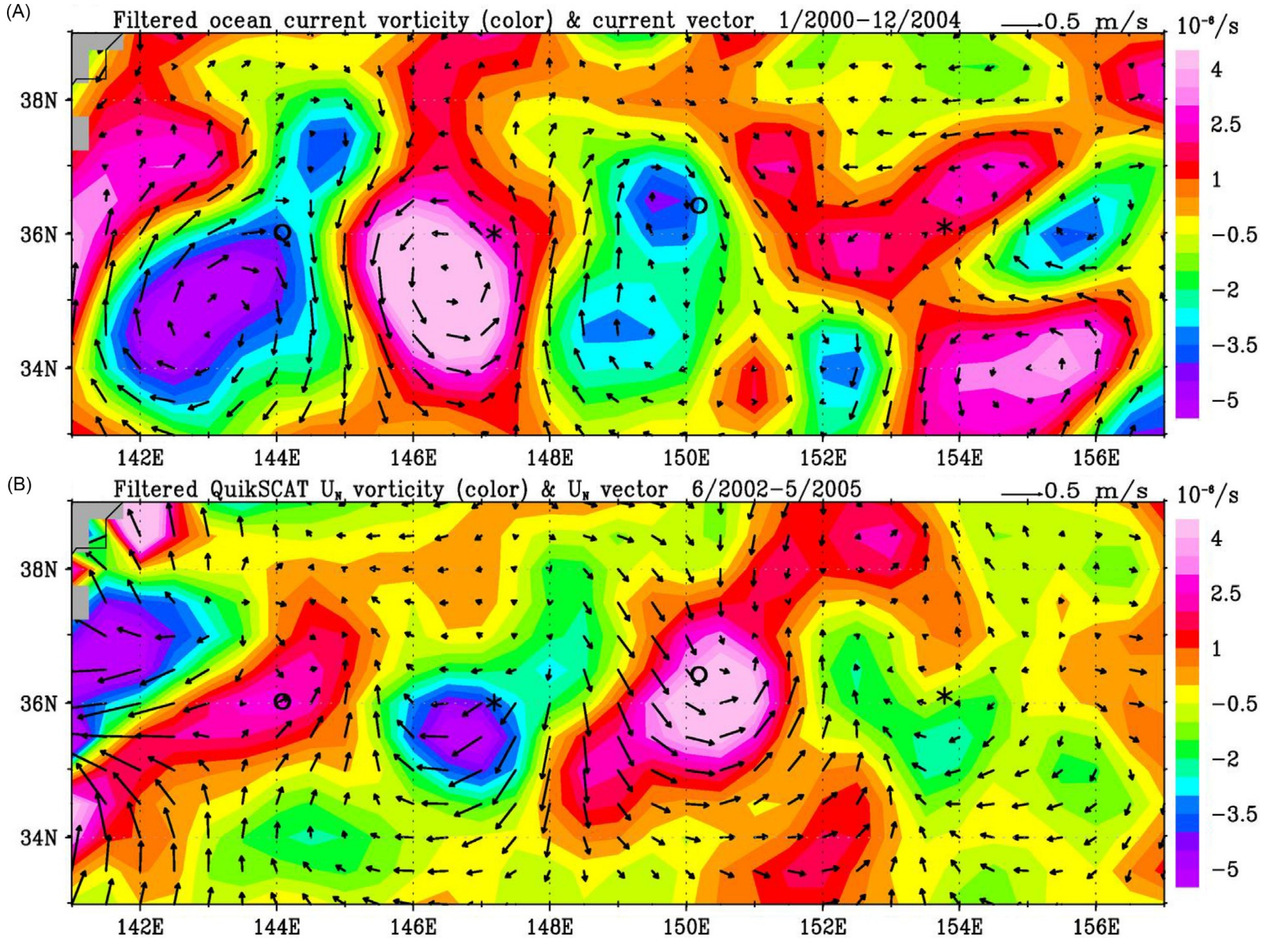

Fig. 4 (A) Filtered vector (*black arrows*) superimposed on vorticity (color, 10^{-6}/s) of the surface current measured by Lagrangian drifters. (B) Filtered vector (*black arrows*) superimposed on vorticity (color, 10^{-6}/s) of QuikSCAT U_N.

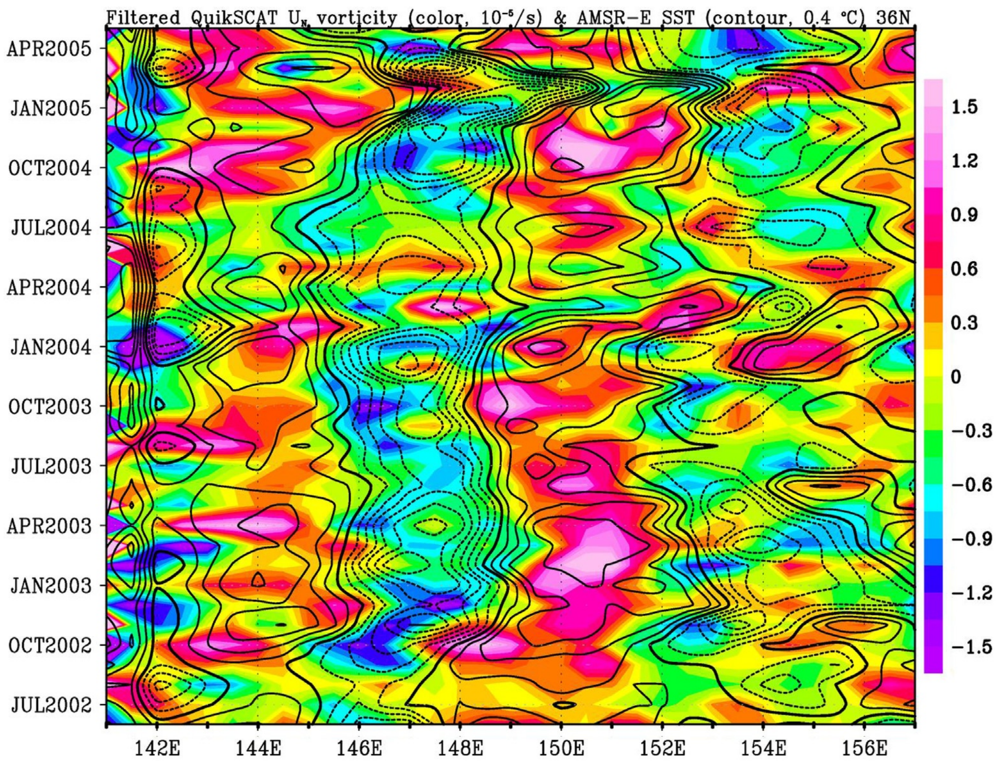

Fig. 5 Time–longitude variations of filtered U_N vorticity (color, 10^{-5}/s) and SST isotherm (0.4°C interval) at 36°N.

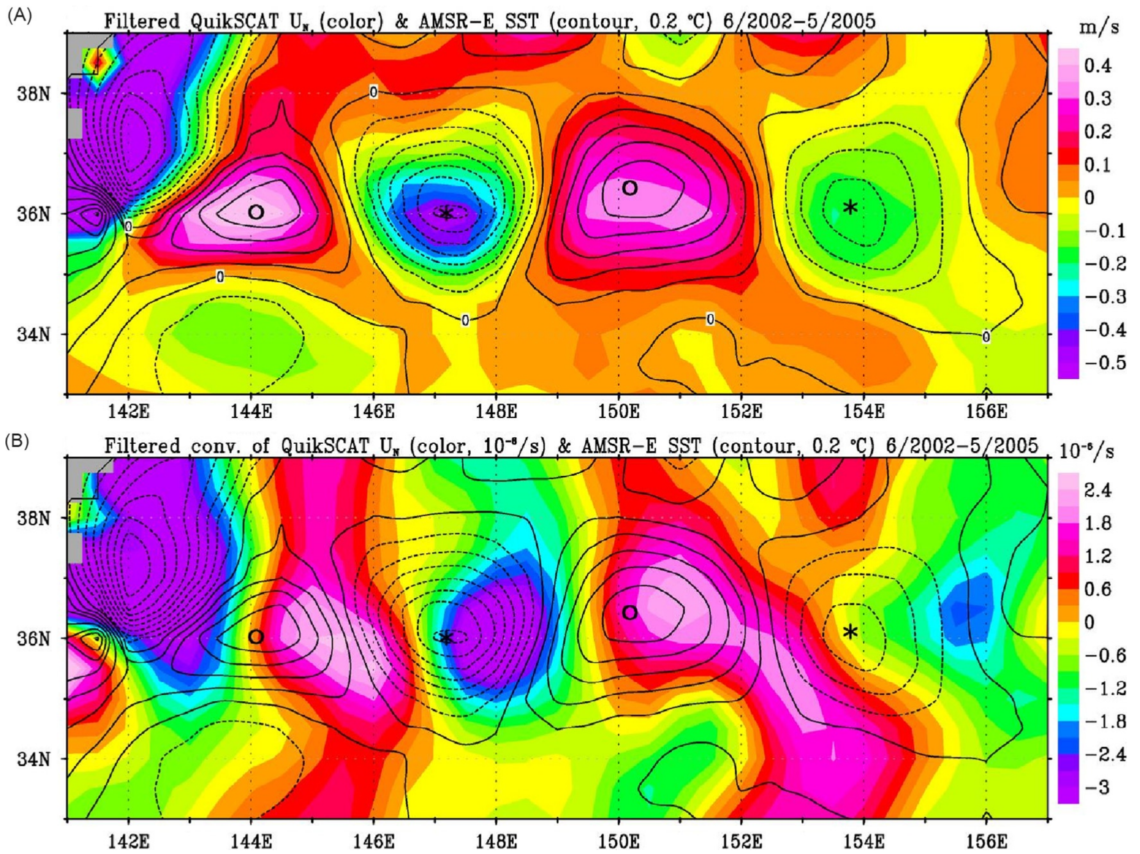

Fig. 6 Maps of filtered (A) magnitude of U_N (color) superimposed by SST isotherm (0.2°C interval), and (B) U_N convergence (color, 10^{-6}/s), superimposed by SST isotherms (0.2°C interval), averaged from June 2002 to May 2005.

conditions, e.g., western boundary currents, Circumpolar Current, marginal seas during cold air outbreak, warm and cold ocean eddies, intertropical convergence zone, and typhoon wake.

Fig. 6A shows the spatial coherence between SST and U_N, with filtering similar to that applied to data in Fig. 4. High magnitudes of U_N are found over warm water and low magnitudes are found over cool water. The convergence/divergence centers are in quadrature, located at the steepest U_N gradient in downwind direction, as shown in Fig. 6B. The circles and crosses mark the location of high and SST centers. Turbulence generated by buoyancy cause stronger stress and latent heat flux over warm water, and weaker flux over cold water. The surface turbulent fluxes are independent to the variation of other atmospheric forcing and (see "Relating Wind and Stress" section), therefore, the coherence is ubiquitous. Fig. 7 shows that the monthly variation of divergence center is consistently related to SST centers.

To demonstrate more clearly the SST-induced divergence and vorticity distribution, a conceptual experiment was performed. A uniform wind field at 10 m high is assumed to blow from west to east over the eddies, which is the average wind for the region for the same period of QuikSCAT observations, provided by the operational products of the European Center for Medium-range Forecast (ECMWF). Surface U_N is computed using the bulk parameterization model of Liu et al. (1979) based just on similarity formulation of surface layer turbulence transport. By definitions, divergence $= \partial\tau_x/\partial x + \partial\tau_y/\partial y$ and vorticity $= \partial\tau_y/\partial x - \partial\tau_x/\partial y$, where τ_x and τ_y are the zonal and meridional components of stress. Without meridional component, the divergence and vorticity centers are located at the highest zonal gradient and meridional gradient of stress respectively. Fig. 8 clearly shows the downwind convergence and crosswind vorticity distribution, as inherent with warm and cold eddies, without involving boundary layer dynamics above.

Stress feedback to the combined effect of current and temperature in mesoscale eddies remain to be characterized. As we move up from the constraint of the surface, other boundary layer forces, such as pressure gradient and Coriolis forces become important and the centers of divergence and vorticity of wind will be located at different places from those of surface stress as discussed by Liu and Xie (2014), Wang and Liu (2015), and others. The difference between wind and stress distribution has been obscured in the operational products of NWP. NWP centers have been assimilating scatterometer measurement as 10 m wind, and the distribution of the wind product follows the distribution scatterometer measurements.

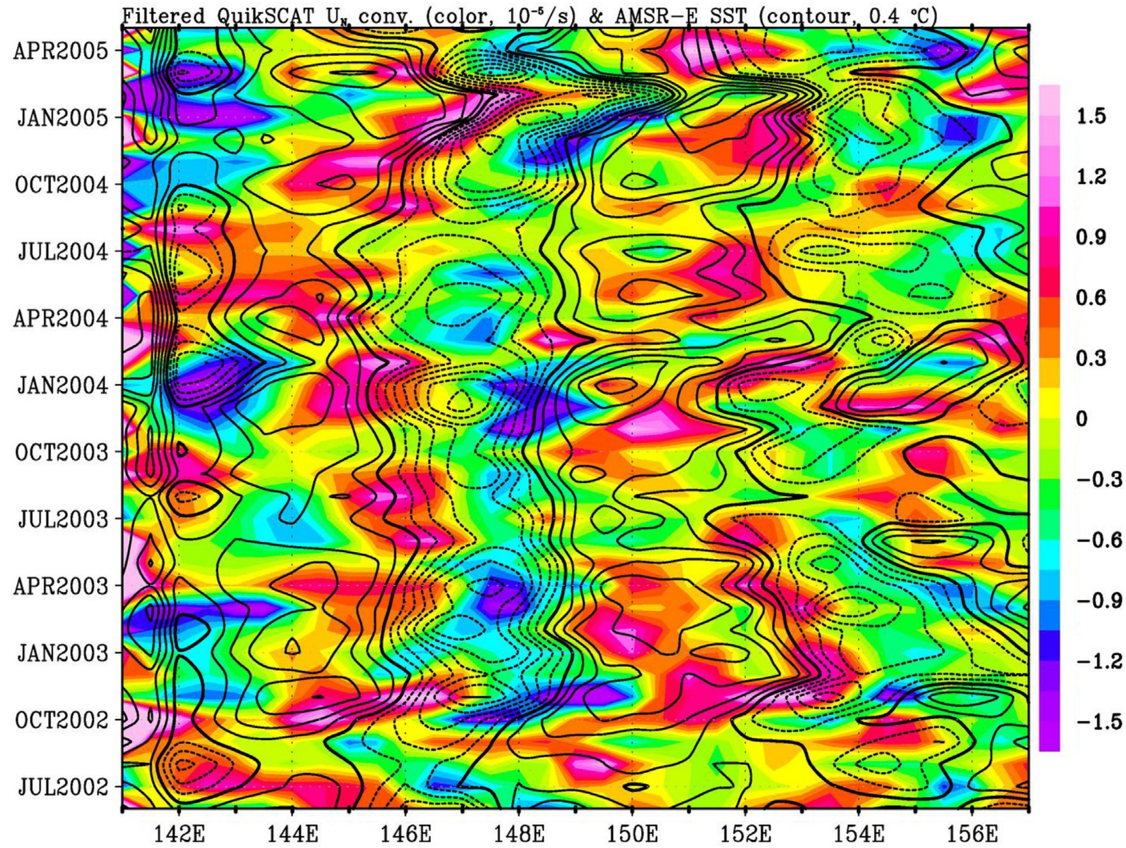

Fig. 7 Time–longitude variations of filtered U_N convergence (color, 10^{-5}/s) superimposed by SST isotherms (0.4°C interval) at 36°N.

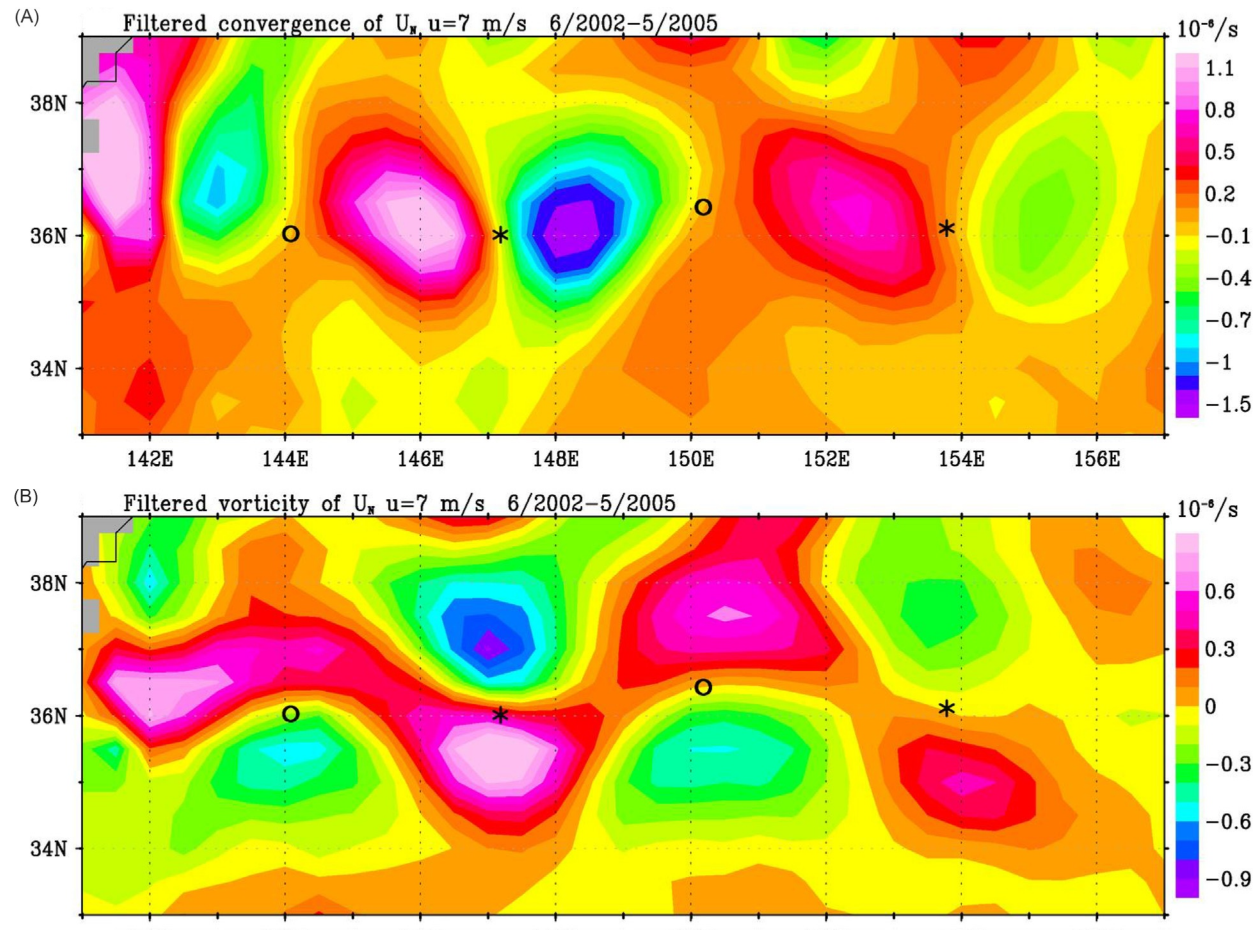

Fig. 8 (A) Convergence, and (B) vorticity of filtered U_N computed from a uniform wind field of 7 m/s (unit is 10^{-6}/s).

Implication and Future Study

Although most oceanographers recognize surface stress as the driver of ocean circulation and scatterometers have the unique capability of measuring stress, they are still deriving stress from winds retrieved from the scatterometer. NWP centers are still assimilating scatterometer observations as 10 m winds. The scatterometer has been considered as an atmospheric sensor and its priority in competing for limited resources is traditionally decided by atmospheric panels. As illustrated in "Under Tropical Cyclone" and "Over Ocean Fronts and Eddies" sections, stress is an ocean parameter no less than an atmospheric parameter, and oceanographers should set national and international priority of scatterometer deployments.

The stress-measuring capability of the scatterometers exposes the need of new investigations. If stress increases much slower than wind in TC, how is the reduction in surface drag and ocean mixing affect the intensification of TC? How are the strong wind gradients in the inner core of TC reflected in the air–sea transfer? With the effects of ocean circulation and temperature on stress over mesoscale eddies, how does the combined feedback changes ocean circulation and vertical transport by the eddies?

The inner core of the TC is often obscured by rain from Ku-band scatterometers. C-band is only slightly better than Ku-band in mitigating rain effect. L-band sensors, however, are much less influenced by rain attenuation. There are several U.S. missions that have L-band sensors for wind retrieval (Yueh et al., 2013). The L-band signals are sensitive to ocean surface waves with longer wavelengths than the short waves that affect C-band and Ku-band signals and the mechanism on how these waves interact with stress needs further studies.

The space agencies in Europe, India, and China plan to maintain C-band and Ku-band scatterometers for operational applications. The India Space Agency (ISRO) plans to continue Scatsat series and the European Agency Eumetsat plans to launch ASCAT-C in 2018. New technology is being developed for polarimetric radiometer following WindSat. A low cost and compact Compact Ocean Wind Vector Radiometer (COWVR) will be deployed by the Department of Defense in 2017 (Brown et al., 2014).

Acknowledgments

This study was performed at the Jet Propulsion Laboratory, California Institute of Technology under contract with the National Aeronautics and Space Administration (NASA). It was supported by the Physical Oceanography and Cyclone Global Navigation Satellite System programs of NASA.

References

Bell MM, Montgomery MT, and Emanuel KA (2012) Air–sea enthalpy and momentum exchange at major hurricane wind speeds observed during CBLAST. *Journal of Atmospheric Science* 69: 3197–3222. http://dx.doi.org/10.1175/JAS-D-11-0276.1.
Brown GS (1978) Backscattering from a Gaussian-distributed perfectly conducting rough surface. *IEEE Transactions on Antennas and Propagation* AP-26: 472–482.
Brown RA and Liu WT (1982) An operational large-scale marine planetary boundary layer model. *Journal of Applied Meteorology* 2: 261–269.
Brown S, Focardi P, Kitiyakara A, Maiwald F, Montes O, Padmanabhan S, Redick R, Russell D, and Wincentsen J (2014) The compact ocean wind vector radiometer: A new class of low-cost conically scanning satellite microwave radiometer system. In: *American Meteorological Society Annual Meeting*.
Chelton DB, Esbensen SK, Schlax MG, Thum N, Freilich MH, Wentz FJ, Gentemann CL, McPhaden MJ, and Schoff PS (2001) Observations of coupling between surface wind stress and sea surface temperature in the eastern tropical Pacific. *Journal of Climate* 14: 1479–1498.
Donelan MA, Haus BK, Reul N, Plant WJ, Stiassnie M, Graber HC, Brown OB, and Saltzman ES (2004) On the limiting aerodynamic roughness of the ocean in very strong winds. *Geophysical Research Letters* 31:L18306. http://dx.doi.org/10.1029/2004GL019460.
Duhaut THA and Straub DN (2006) Wind stress dependence on ocean surface velocity: Implications for mechanical energy input to ocean circulation. *Journal of Physical Oceanography* 36: 202–211.
Emanuel K (1995) Sensitivity of tropical cyclones to surface exchange coefficients and a revised steady state model incorporating eye dynamics. *Journal of Atmospheric Science* 52: 3969–3976.
Esteban-Fernandez D, Carswell JR, Frasier S, Chang PS, Black PG, and Marks FD (2006) Dual-polarized C- and Ku-band ocean backscatter response to hurricane-force winds. *Journal of Geophysical Research* 111:C08013. http://dx.doi.org/10.1029/2005JC003048.
Fois F, Hoogeboom P, Le Chevalier F, and Stoffelen A (2015) Future ocean scatterometry: On the use of cross-polar scattering to observe very high winds. *IEEE Transactions on Geoscience and Remote Sensing* 53: 5009–5020. http://dx.doi.org/10.1109/TGRS.2015.2416203.
French JR, Drennan WM, Zhang JA, and Black PG (2007) Turbulent fluxes in the hurricane boundary layer. Part I: Momentum flux. *Journal of Atmospheric Science* 64: 1089–1102. http://dx.doi.org/10.1175/JAS3887.1.
Hogg A, Dewar MCWK, Berloff P, Ktavsgtov S, and Huchinson DK (2009) The effect of mesoscale ocean-atmosphere coupling on the large-scale ocean circulation. *Journal of Climate* 22: 4066–4082.
Holthuijsen LH, Powell MD, and Pietrzak JD (2012) Wind and waves in extreme hurricanes. *Journal of Geophysical Research* 117:C09003. http://dx.doi.org/10.1029/2012JC007983.
Jarosz E, Mitchell DA, Wang DW, and Teague WJ (2007) Bottom-up determination of air-sea momentum exchange under a major tropical cyclone. *Science* 315: 1707–1709. http://dx.doi.org/10.1126/science.1136466.
Jones WL and Schroeder LC (1978) Radar backscatter from the ocean: Dependence on surface friction velocity. *Boundary Layer* 13: 133–149.
Kelly KA, Dickensen S, McPhaden MJ, and Johnson GC (2001) Ocean currents evident in satellite wind data. *Geophysical Research Letters* 28: 2469–2472.
Large WG and Pond S (1981) Open ocean momentum flux measurements in moderate to strong winds. *Journal of Physical Oceanography* 11: 324–336.
Liu WT (2002) Progress in scatterometer application. *Journal of Oceanography* 58: 121–136.
Liu WT and Large WG (1981) Determination of surface stress by Seasat-SASS: A case study with JASIN Data. *Journal of Physical Oceanography* 11: 1603–1611.
Liu WT and Tang W (1996) *Equivalent neutral wind*. Pasadena: Jet Propulsion Laboratory. JPL Publication 96-17, 16 pp.
Liu WT and Tang W (2016) Relating wind and stress under tropical cyclones with scatterometer. *Journal of Atmospheric and Oceanic Technology* 33: 1151–1158. http://dx.doi.org/10.1175/JTECH-D-16-0047.1.

Liu WT and Xie X (2006) Measuring ocean surface wind from space. In: Gower J (ed.) *Remote sensing of the marine environment, manual of remote sensing*. 3rd edn., vol. 6, pp. 149–178, Bethesda, MD: American Society for Photogrammetry and Remote Sensing. Chapter 5.
Liu WT and Xie X (2008) Ocean-atmosphere momentum coupling in the Kuroshio Extension observed from Space. *Journal of Oceanography* 64: 631–637.
Liu WT and Xie X (2013) Sea surface wind/stress vector. In: Njoku E (ed.) *Encyclopedia of remote sensing*. New York: Springer. http://dx.doi.org/10.1007/SpringerReference_327232.
Liu WT and Xie X (2014) Ocean-atmosphere coupling over mid-latitude ocean fronts observed from space. Key-note presentation. In: *Proc. Eumetsat Conf., Geneva*. 9 pp, http://airsea.jpl.nasa.gov/publication/paper/Liu-Xie-Eumetsat.proc-2014.pdf.
Liu WT, Katsaros KB, and Businger JA (1979) Bulk parameterization of air-sea exchanges in heat and water vapor including the molecular constraints at the interface. *Journal of Atmospheric Science* 36: 1722–1735.
Liu WT, Xie X, Polito PS, Xie S, and Hashizume H (2000) Atmosphere manifestation of tropical instability waves observed by QuikSCAT and Tropical Rain Measuring Missions. *Geophysical Research Letters* 27: 2545–2548.
Liu WT, Xie X, and Niiler PP (2007) Ocean-atmosphere interaction over Agulhas Extension Meanders. *Journal of Climate* 20(23): 5784–5797.
Liu WT, Xie X, and Tang W (2010) Scatterometer's unique capability in measuring ocean surface stress. In: Alberotanza L, Barale V, and Gower JFR (eds.) *Oceanography from space*, pp. 93–111, New York: Springer.
Pacanowski RC (1987) Effect of surface current in surface stress. *Journal of Physical Oceanography* 17: 833–838.
Park K-A, Cornillon P, and Codiga DL (2006) Modification of surface winds near ocean fronts: Effects of the Gulf Stream rings on scatterometer (QuikSCAT, NSCAT) wind observations. *Journal of Geophysical Research* 111:C03021. http://dx.doi.org/10.1029/2005JC003016.
Powell MD, Houston SH, Amat LR, and Morisseau-Leroy N (1998) The HRD real-time hurricane wind analysis system. *Journal of Wind Engineering & Industrial Aerodynamic* 77&78: 53–64.
Powell MD, Vickery PJ, and Reinhold TA (2003) Reduced drag coefficient for high wind speeds in tropical cyclones. *Nature* 422: 279–283. http://dx.doi.org/10.1038/nature01481.
Smith SD (1980) Wind stress and heat flux over the ocean in gale force winds. *Journal of Physical Oceanography* 10: 709–726.
Soloviev A, Lukas R, Donelan M, Haus B, and Ginis I (2014) The air-sea interface and surface stress under tropical cyclones. *Nature Scientific Reports*. http://dx.doi.org/10.1038/srep05306.
Wang Y-H and Liu WT (2015) Observational evidence of frontal-scale atmospheric responses to Kuroshio Extension variability. *Journal of Climate* 28: 9459–9472. http://dx.doi.org/10.1175/JCLI-D-14-00829.1.
Wright JW (1968) A new model for sea clutter. *IEEE Transactions on Antennas and Propagation* AP-16: 217–233.
Xie S-P, Ishiwatari M, Hashizume H, and Takeuchi K (1998) Coupled ocean-atmospheric waves on the equatorial front. *Geophysical Research Letters* 25: 3863–3866.
Yueh SH, Tang W, Fore AG, Neumann G, Hayashi A, Freedman A, Chaubell J, and Lagerloef GSE (2013) L-band passive and active microwave geophysical model functions of ocean surface winds and applications to Aquarius retrieval. *IEEE Transactions on Geoscience and Remote Sensing* 51: 4619–4631.